The role of North Brazil Current transport in the paleoclimate of the Brazilian Nordeste margin and paleoceanography of the western tropical Atlantic during the late Quaternary

Trevor E. Nace [a], Paul A. Baker [ab], Gary S. Dwyer [a], Cleverson G. Silva [b], Catherine A. Rigsby [bc], Stephen J. Burns [d], Liviu Giosan [e], Bette Otto-Bliesner [f], Zhengyu Liu [g], Jiang Zhu [g],

[a]Division of Earth and Ocean Sciences, Duke University, Durham, NC 27708 USA
[b]Departamento de Geologia, Universidade Federal Fluminense, Niterói, RJ, Brazil
[c]Department of Geological Sciences, East Carolina University, Greenville, NC 27858 USA
[d]Department of Geosciences, University of Massachusetts, Amherst, MA 01003 USA
[e]Woods Hole Oceanographic Institution, Woods Hole, MA 02543
[f]Climate and Global Dynamics, National Center for Atmospheric Research, Boulder, CO, 80307 USA
[g]Department of Atmospheric and Oceanic Sciences, University of Wisconsin, Madison, WI 53706, USA

Corresponding author: Paul A. Baker

Address:
Professor Paul A. Baker
Duke University
Division of Earth and Ocean Sciences
Box 90227
Durham, NC 27708-0227 USA

Phone: 1-919-684-6450
Email: pbaker@duke.edu

ABSTRACT

Reconstructions of surface paleoceanographic conditions of the western equatorial Atlantic and past climates of the adjacent Northeast Brazilian (the "Nordeste") continental margin were undertaken by analyzing sediments from a piston core and associated gravity and box cores recovered from 3107 meter water depth at 0° 20′ N on the equatorial Brazilian continental slope. The record is dated by radiocarbon analysis and oxygen isotopic stratigraphy of planktonic foraminifers and spans from near-modern to approximately 110 Ka.

High-resolution XRF analysis provides insight into the paleoclimate history of the Nordeste during the last glacial interval. Several large-amplitude and abrupt peaks are observed in the time series of Ti/Ca and are usually accompanied by peaks of Fe/K. Together these record periods of increased precipitation and intense weathering on the adjacent continent and increased terrestrial sediment discharge from Nordeste rivers into the Atlantic. Within the limits of dating accuracy, most Ti/Ca peaks correlate with Heinrich events in the North Atlantic. This record thus corroborates, and extends back in time, the previous record of Arz et al (1998) determined on sediment cores from farther southeast along the Nordeste margin.

Stable oxygen isotopic analysis and Mg/Ca paleothermometry on the near-surface-dwelling planktonic foraminiferal species Globierinoides ruber find that mean sea-surface temperature (SST) during glacial time (20 to 55 Ka, n = 97) was 23.89 ± 0.79 °C and the mean SST during the late Holocene (0 to 5 Ka, n = 14) was 26.89 ± 0.33 °C. SSTs were 0.5 to 2 °C higher and inferred sea-surface salinities were lower during most

of the periods of elevated Ti/Ca, thus, as observed in previous studies, the western equatorial Atlantic was warm (at least locally) and the adjacent southern tropical continent was wet at the same time that the high-latitude North Atlantic was cold.

Using the SYNTRACE-CCSM3 fully coupled climate model with transient forcing for the period 22 Ka to present, we find that decreased transport of the North Brazil Current co-occurs with reduced Atlantic meridional overturning circulation, and colder-than-normal SSTs in the North Atlantic region. These simulated conditions are invariably associated with significantly increased precipitation in the Nordeste region.

KEYWORDS

North Brazil Current; Amazon margin; late Quaternary; Heinrich events

1. INTRODUCTION

Greenland ice cores (e.g., Dansgaard et al., 1993 and Grootes et al., 1993) and North Atlantic sediment cores (e.g., Heinrich, 1988 and Bond and Lotti, 1995) distinguish the late Quaternary as a period of abrupt, large amplitude oceanic and atmospheric reorganizations, the Dansgaard-Oeschger and Heinrich events. These events seem to have strongly impacted South and Central American paleoclimate. In the northern neotropics, for example at Lake Peten-Itzá (Hodell et al., 2008) and on the Venezuelan continental margin (Peterson et al., 2006), North Atlantic cold events (we will call them "NACE" events and refer to them as occurring at a variety of timescales), such as Heinrich events, were associated with dry conditions. South of the equator, NACE events were associated with increased precipitation and runoff in the Andes (e.g., Baker et al., 2001a and b, Fritz et al., 2010, Kanner et al., 2012 and Cheng et al., 2013), the Amazon (Wang et al., 2014), and the Brazilian Nordeste (e.g., Arz et al., 1998, Wang et al., 2004 and Cruz et al., 2009). Many climate simulations associate NACE events with decreased Atlantic meridional overturning circulation (AMOC) (e.g., Vellinga and Wood, 2002, Zhang and Delworth, 2005, Broccoli et al., 2006, Liu et al., 2009, and Zhang et al., 2011) and a southward shift of the ITCZ and its defining belts of wind and precipitation (e.g., Chiang et al., 2003 and Vellinga and Wu, 2004).

Zhang et al. (2011), using both modern instrumental observations and coupled ocean-atmosphere climate simulations, concluded that North Brazil Current (NBC) transport is correlated with North Atlantic SST (i.e., the Atlantic multi-decadal

oscillation, AMO) and AMOC transport on decadal timescales. On the basis of our sediment record and our model simulations, we suggest that a similar relation held on centennial and millennial timescales during glacial stages--decreased northward cross-equatorial heat transport during NACE events was associated with decreased AMOC, increased western equatorial Atlantic SST, and increased precipitation on the adjacent continent.

2. STUDY AREA

Core CDH 86 (00° 20.002' N, 44° 12.544' W, 3107 m water depth, 30.55 m total length) was retrieved in February 2010 during an oceanographic expedition of the R/V Knorr (KNR 197-4) to the Brazilian continental margin offshore the mouth of the Amazon River. The coring site was located on the continental slope, 190 km from the modern coastline and 430 km north of the mouth of the Parnaíba River (Fig. 1). Core CDH 86 was collected from a continuous, conformable sediment sequence as verified by high-resolution 3.5 kHz seismic reflection survey. In addition to the piston core, a box core (BC 82 from 00° 20.266' N, 44° 12.541' W, 3113 m water depth, 89 cm total length) and a gravity core (GGC 81 from 00° 20.260' N, 44° 12.570' W, 3116 m water depth, 3.99 m total length) were also collected at the same site to ensure recovery of the uppermost sediment section.

Modern terrigenous sediment reaching this site is expected to originate by northward transport by the NBC from fluvial sources in the northern Nordeste region of Brazil, the most important of which today is the Parnaíba River. This river has a modern drainage basin area of about 344,000 km^2 (approximately 5% that of the Amazon River

drainage basin) (Marques et al. 2004). Average precipitation in this region is 1730 mm a^{-1} and evapotranspiration averages about 1500 mm a^{-1} (Marques et al. 2004). The annual average discharge rate of the Parnaíba River is 1272 m^3 s^{-1}, with peak flows in February and March and lowest flow in July and August (Marques et al. 2004). Sedimentary sequences in the Parnaíba Basin range from early Devonian to Cretaceous (Bigarella et al. 1965); the sediment is deeply weathered and soils of the basin are mostly lateritic oxisols, comprised predominantly of quartz, kaolinite, and iron and aluminum oxides (Volkoff, 1983).

Surface ocean circulation in the study region is dominated by the NBC. As the South Equatorial Current meets the South American continental margin at approximately 10-15° S it bifurcates forming the southward flowing Brazil Current and the northward flowing NBC (Schott et al. 1995 and Stramma et al. 1995). The NBC transports warm saline water from the tropical South Atlantic to the northern hemisphere in a narrow, fast moving, western boundary current. The NBC extends to intermediate water depths (ca. 800 m) where it merges with northward advected Antarctic Intermediate Water (Talley et al., 2011). NBC transport is highly variable, with maximum measured transport of approximately 36 Sv during the austral winter, minimum transport of approximately 13 Sv during the austral fall, and seasonal retroflection into the North Equatorial Countercurrent at 6-7°N from June to January (Johns et al., 1998). Seasonal variability in NBC transport is correlated with north-south migration of the ITCZ, and associated changes in wind stress curl. Mesoscale variability in NBC transport is associated with large anti-cyclonic rings that form as the NBC moves

northward along the coast (Richardson et al., 1994 and Talley et al., 2011). Mean annual SST and sea surface salinity (SSS) at the study site are respectively 27.3°C and 35.7psu (Antonov et al., 2010 and Locarnini et al., 2010).

3. MATERIALS AND METHODS

Cores were continuously analyzed for magnetic susceptibility (MS) with a Bartington sensor installed on a shipboard Geotek logger. Cores were refrigerated and shipped to Woods Hole Oceanographic Institute (WHOI) for storage and subsequent splitting, core description, sampling, and analysis. Sediment chemistry was analyzed at 2 mm intervals on the gravity and piston cores, using an ITRAX X-ray fluorescence (XRF) spectrometer in the Coastal Systems lab at WHOI. The following elements were determined: Si, P, S, Cl, K, Ca, Sc, Ti, V, Cr, Mn, Fe, Co, Ni, Cu, Zn, Ga, Ge, As, Se, Br, Rb, Sr, Zr, Ag, Cd, I, Cs, Ba, Ta, W, Re, Au, Hg, Tl, Pb, U. Elemental ratios only are reported to account for density changes down core and are unitless, as each element is measured in counts per second.

Mixed assemblages of planktonic foraminifers were sieved and picked from the 250-350 μm size range for radiocarbon dating. Eighteen radiocarbon dates were undertaken on these samples. Radiocarbon dates were also undertaken on total organic carbon from seven of the same intervals. Radiocarbon analysis was done at the National Ocean Sciences Accelerated Mass Spectrometer (NOSAMS) Facility, WHOI. Radiocarbon ages were converted to calendar years using the 'Fairbanks0107' calibration (Fairbanks et al., 2005). Foraminifer ages were corrected for marine reservoir effect assuming a constant 400-year reservoir age (Bard, 1998). No local reservoir effects were

considered as little reservoir correction data exist for this region. No reservoir age was added to organic matter dates as the glacial-age sedimentary organic carbon is thought to be primarily derived from a terrestrial source (Eglinton et al., 1997).

Sediment was sampled at 1 cm intervals in the box core and at 10 cm intervals in the gravity and piston cores for foraminifer stable isotopic and minor elemental analyses. Sediment samples were wet sieved and the planktonic foraminifer species *Globigerinoides ruber* (white) was picked from the 350-500 μm size range. Stable isotope measurements were made on a Finnigan Kiel-III automated carbonate preparation device coupled to a Finnigan Delta Plus ratio mass spectrometer in the Department of Geosciences at the University of Massachusetts, Amherst. All values are reported with respect to the standard Vienna Pee-Dee Belemnite (VPDB). Precision is better than 0.1‰ for $\delta^{18}O$. Picked *Globigerinoides ruber* samples were cleaned and prepared for magnesium and calcium analyses using established procedures (Barker et al., 2003), but adding a reductive step to remove oxide contamination. Magnesium and calcium concentrations were measured on a Spectraspan 7 direct current plasma atomic emission spectrometer in the Duke University Division of Earth and Ocean Sciences. Analytical precision on internal standards over the course of this study was 1.7%. A total of 318 unknown samples were analyzed. Sufficient material was present that whole sample replicates were picked, cleaned and analyzed for 235 of these samples. The 235 whole sample replicates yielded a mean error of 4.8%. This degree of reproducibility between completely independent sub-samples suggests that diagenetic alteration and detrital contamination are minimal. SST was calculated from Mg/Ca ratios using the relation of

Anand et al. (2003) from calibration of sediment trap samples in the tropical Atlantic (1000*Mg/Ca=0.38 exp(0.09*T), where T is in °C, and Mg/Ca is a mole ratio. Recent studies have demonstrated that seawater salinity can significantly influence foraminifer Mg/Ca composition (Nürnberg et al., 1996, Ferguson et al., 2008, Kisakurek et al., 2008 and Honisch et al., 2013). Honisch et al. (2013) reported Mg/Ca-sensitivity of 3.3 ± 1.7% per practical salinity unit (psu), considerably lower than found in some previous studies (e.g., Arbuszewski et al., 2010). The expected ~1 psu salinity increase of the last glacial period would thus bias the Mg/Ca-derived SST of glacial samples by approximately +0.3°C.

The $\delta^{18}O_{sw}$ values of ancient seawater were calculated following the methodology of Lea et al. (2000) using the temperature and $\delta^{18}O$ relation derived for *Orbulina universa* (Bemis et al., 1998) of $T=14.9-4.8(\delta^{18}O_c - \delta^{18}O_{sw})$, which was shown to be applicable to *G. ruber* (Thunell et al., 1999) where T is in °C and $\delta^{18}O_c$ is $\delta^{18}O$ of the *G. ruber* shell. The $\delta^{18}O_{sw}$ is reported in per mil relative to the Vienna standard mean ocean water (VSMOW) by subtracting 0.27‰ from the calculated $\delta^{18}O_{sw}$ (Bemis et al., 1998).

4. RESULTS

Radiocarbon ages were determined on the upper 10 m of piston core CDH86, and on gravity core GGC81 and box core BC82. Age tie points between the CDH86 stable oxygen isotopic record and the stacked benthic $\delta^{18}O$ records of Lisiecki and Raymo (LR04) (2005) were used to constrain the age model from 43 to 110 Ka. The age model is based on linear interpolation between selected data points for the entire record, using ^{14}C dates from 0-43 Ka and LR04 age tie points for the remainder of the record

(Fig. 2). The organic carbon ages (uncorrected for marine reservoir age) are 2,000 to 6,000 years older than the reservoir corrected foraminifer ages from the same interval (Fig. 2). Sedimentation rate decreased from an average value of 33 cm/kyr during the glacial to an average of 3 cm/kyr, typical of pelagic sedimentation rates, during the Holocene.

We use the Ti/Ca ratio as an indicator of the relative magnitude of the terrestrial contribution to the marine sediment record (Arz et al., 1998 and Jennerjahn et al., 2004) that should be closely tied to effective moisture (precipitation minus evapotranspiration) on the adjacent continent. This interpretation partly hinges upon the assumption that calcium fluxes remained reasonably constant throughout the record. Calcium in this setting is largely derived from biogenic $CaCO_3$ shell material (mostly pteropods, foraminifers, and calcareous nannoplankton). Three factors typically affect $CaCO_3$ concentration in marine sediments: biological production, dissolution, and dilution by non-carbonate sediments. In the present case, neither changes of the rate of production nor the rate of dissolution seem to have significantly affected these sediments. Ruhlemann et al. (1996) found that paleoproductivity in the western equatorial Atlantic, proximal to the Nordeste, was low and constant throughout the time period represented by most of our record. Our scanning electron microscopic examination of several foraminifer tests indicates that diagenetic carbonate overgrowth is not significant throughout the core. The presence of aragonitic pteropods throughout the core suggests that dissolution in the water column or on the seafloor was minimal. Finally, the observed changes of Ti/Ca ratio are so large and abrupt (Fig. 3) that it seems

most unreasonable that these could be brought about by either productivity or dissolution changes. Taken together, we conclude that changes in calcium concentrations are most likely due to dilution of biogenic $CaCO_3$ by terrestrial detrital sediment, thus that Ti/Ca in this core is a trustworthy indicator of terrigenous sediment input and continental runoff.

Throughout the record Ti/Ca values remain low except when interrupted by 15 to 20 abrupt peaks that range from a few hundred to 5000 years duration (represented by ~10 to 150 cm thick sediment intervals in the core) (Fig. 3). These events occur throughout the entire glacial portion of our record, and most correspond with low (i.e. cold) $\delta^{18}O$ intervals in the Greenland ice cores (NGRIP, 2004 and Svensson et al., 2008). Ti/Ca peaks in our record are well correlated with well-dated (Obrochta et al., 2012 and 2014) Heinrich events H1 through H6 (Fig.3), although H2 is represented by only a minor peak in our record (surprisingly so, as H2 is well recorded farther south (Arz et al., 1998).

Today, sediment and water discharged from the Parnaíba River and other rivers of the northern Nordeste are entrained in the North Brazil Current and advected northwestward along the inner continental shelf. During sea-level lowstands of the glacial period, however, these rivers, like the Amazon itself farther to the north, incised the continental shelf and debouched directly onto the upper continental slope. Increased precipitation in the northern Nordeste, possibly as a result of higher SST offshore, would have increased the intensity of physical weathering on the landscape, the riverine discharge and suspended sediment load at the river mouths, and the

suspended sediment flux at the study site. Thus, we interpret increase in precipitation in the northern Nordeste as the underlying cause of the observed Ti/Ca peaks. That the Ti/Ca peaks in our record correspond so well with the timing and relative magnitude of the Ti/Ca peaks from significantly farther south (03°40.09' S, 37°43.09' W, 767 m water depth, Arz et al., 1998) indicates that the spatial footprint of these centennial to millennial precipitation changes extended throughout the entire Nordeste region of Brazil (e.g., Cruz et al., 2009) and far beyond (e.g., Kanner et al., 2012, Cheng et al., 2013 and Wang et al., 2014).

Stuut et al. (2005) and Mulitza et al. (2008) previously demonstrated the utility of Fe/K in Atlantic sediment cores as a measure of aridity in the adjacent Sahel region of North Africa. In the tropics, wet conditions increase the intensity of chemical weathering and can lead to higher concentrations of iron in soils and detrital sediments (originally precipitated as insoluble iron oxy-hydroxides) compared to more soluble and mobile potassium. Thus Mulitza et al. (2008) concluded that rapid decreases in Fe/K in terrigenous sediments indicated drier conditions in the Sahel during Heinrich events of the past ~60 Ka.

In our record, most Ti/Ca peaks correspond to peaks in Fe/K (Fig. 4). However, the nature of both curves appears to evolve from MIS 5 into the full glacial conditions that followed. Numerous Ti/Ca peaks, both large and small, characterize the early part of the record from 112 to 60 Ka. It is not likely that these early Ti/Ca peaks were associated with true Heinrich events, but they do likely represent wet periods in the Nordeste region. Most of the Ti/Ca peaks of this period are accompanied by Fe/K peaks,

but the Fe/K peaks in this period tend to be much longer lived. Perhaps this signifies generally wetter conditions and deeper weathering on the continent during most of MIS 5. After 60 Ka, the Ti/Ca peaks are "canonical" in the sense that they are abrupt and distinct; each Ti/Ca peak of this later period is paired with a distinct Fe/K peak; each Ti/Ca peak is also paired with a Heinrich event. For both proxies, the events of MIS 4 between 70 and 60 Ka, stand out as unusually long in duration and large in amplitude. Fe/K presages this period with a slow increase beginning ca 75 Ka leading to an abrupt jump of Ti/Ca ca 64 Ka. Both proxies retain high values for the next ca. 5000 years, a period that coincides with H6 of the North Atlantic. MIS 4 is not only one of the longest-lived and coldest stages of the past 100 kyr in the North Atlantic region, it also appears to be the longest lived wet period in this part of tropical South America. Much later in the record, it is interesting to note that although the YD is marked by only a minor Ti/Ca peak, the wet character of the YD in the southern tropics is borne out by the very pronounced peak of Fe/K.

Principal component analysis (PCA) was carried out using the XRF elemental dataset (13 variables and 15,379 measurements). The first two components account for 49.2% of the total variability (Fig. 5). The first component accounts for 26.1% of the variability, and the main loadings are with Fe and Zr (terrestrial) on the positive end and Ca and Sr (marine) on the negative end. Thus, this first component can be associated with terrigenous versus pelagic provenance. The second component accounts for 23.1% of the variability and is controlled by a suite of elements, most notably K and Si. Of note is the lack of grouping of terrigenous elements (Fe, Ti, K), suggesting their fractionation

by physical or chemical weathering processes. The more mobile K species responds very differently than less mobile Fe, confirming the added value of Fe/K as a tracer for weathering (Mulitza et al., 2008).

Magnetic susceptibility (MS) is a qualitative measure of the fraction of iron bearing minerals, particularly magnetite, in sediment. Magnetite has ~1000 times higher MS than goethite and hematite (Maher and Thompson, 1995), thus oxidative weathering greatly impacts the MS of sediment. Disparities in chemical speciation of Ti versus Fe during weathering may explain the observed anticorrelation between Ti/Ca and MS in our record. Soils in the Parnaíba Basin are primarily lateritic oxisols, in which magnetite has been oxidized to goethite and hematite and is largely associated with the clay fraction (Volkoff, 1983). Titanium in lateritic soils is often found in heavy mineral oxides, most commonly rutile (Weaver, 1976). Soil erosion during wet periods might be expected to physically entrain rutile and some low-MS, ferric oxides and oxy-hydroxides whereas a great amount of iron oxide would remain on the landscape in insoluble form. Thus, in most cases in CDH 86, MS minima coincide with the Ti/Ca maxima (Fig. 6), enforcing the notion that these maxima represent periods of high effective moisture and deep weathering on land. Both ratios decrease with the onset of the Holocene and the transition from a hemi-pelagic to a pelagic depositional environment at the core site.

One of the most obvious characteristics of the Mg/Ca-derived SST (hereafter, SST) record is its large scatter during glacial times. This is not an analytical issue as our whole sample replicates (completely independent samples except that they were taken from the same sample interval) yield very similar values. Rather is seems most likely

that ocean surface conditions (SST and SSS) offshore the present-day mouth of the Amazon (but 4° south of the glacial-age mouth at the shelf edge) were highly spatially variable on all time scales. Nevertheless, throughout MIS 3-5, SST maxima generally align with peaks in Ti/Ca (Fig. 7). The mean SST during glacial time (20-55 Ka, n = 97) was 23.89 ± 0.79°C and during the late Holocene (0 to 5 Ka, n = 14) was 26.89 ± 0.33°C. After a period of elevated SST nearly coincident with the Bolling-Allerod, SST fell during the YD to a near-LGM value of ~23°C at 12.3 Ka. SST again began to rise during the late deglacial period to reach near-modern values of ~27°C by 5 Ka.

Ice volume has a significant influence on both $\delta^{18}O_{sw}$ and salinity (e.g., Dwyer et al., 1995). After accounting for the influence on isotopic composition of both temperature-dependent fractionation and ice volume (Bintanja et al., 2005), the residual, ice volume-corrected $\delta^{18}O_{swivc}$ serves as a proxy for local SSS. Despite the considerable scatter, in most, but not all, cases Ti/Ca peaks coincide with low values of $\delta^{18}O_{swivc}$ signifying low SSS (Fig.8). Only the major Ti/Ca event between 59-64 Ka lacks a corresponding $\delta^{18}O_{swivc}$ minimum—even the small Younger Dryas Ti/Ca peak has a counterpart $\delta^{18}O_{swivc}$ minimum despite the higher sea level, thus more distant river mouth, at that time.

5. DISCUSSION

The study site is supplied with terrigenous sediment believed to be derived from the northern Nordeste region of continental South America. Precipitation in the northern Nordeste during the instrumental period has long been related to, and is well correlated with, oceanographic conditions offshore (e.g., Hastenrath and Heller, 1977,

Hastenrath, 1991, Ward and Folland, 1991 and Nobre and Shukla, 1996). The majority of annual rainfall in the northern Nordeste occurs in March and April, when the ITCZ annually reaches its southernmost position. Meridional variability of the ITCZ is associated with changes in the tropical Atlantic SST gradient that steer cross-equatorial wind anomalies from the cooler to the warmer hemisphere (Nobre and Shukla, 1996). Periods of anomalous warmth in the northern tropical Atlantic often result in early withdrawal of the ITCZ northward bringing about drought conditions in the northern Nordeste. Likewise, anomalously warm conditions in the southern tropical Atlantic tend to delay the northward migration of the ITCZ and generate wetter-than-normal conditions in the northern Nordeste. These precipitation anomalies can occur on a variety of timescales including intra-annual (e.g., Marengo et al., 2008 and Lewis, et al., 2010), decadal (e.g., Hastenrath and Heller, 1977 and Nobre and Shukla, 1996), and, perhaps, centennial/millennial (e.g., Cruz et al., 2009 and this paper). Thus, we posit that the centennial-millennial detrital-rich intervals represented by the Ti/Ca peaks were produced by centennial-millennial increases of regional rainfall that coincided with a cooler northern tropical Atlantic, warmer southern tropical Atlantic, and an anomalously southward-displaced mean position of the ITCZ.

The SST record exhibits both local and global oceanographic forcing throughout the past 110 kyr. SSTs begin to rise from glacial to modern values ca. 12 Ka and only reached modern SSTs ca 5 Ka, much later than northern hemisphere warming indicated by Greenland ice sheets (Dansgaard et al., 1993 and Grootes et al., 1993), where the largest deglacial warming occurs at the onset of the Bolling-Allerød at ~14.7 Ka. In their

study site at 4°S, several hundred kilometers south of this study site, Weldeab et al. (2006) found the largest glacial-to-interglacial transition at the onset of Heinrich 1. The initial warming during Heinrich 1 in the Weldeab record was followed by a slow steady increase to modern SST at 10 Ka, much earlier than the warming seen in our record. This transition of SST from LGM to Holocene likewise differs considerably from the early and steady rise observed in the South Atlantic (Sachs et al., 2001).

Arz et al. (1998) analyzed sediment cores raised from the Nordeste continental margin in the vicinity of 4°S and ascribed Ti/Ca and Fe/Ca peaks to wet phases in the Nordeste that they correlated with Heinrich events. On the basis of oxygen isotopic analysis of planktonic foraminifers, they concluded that the wet events coincided with warm SSTs in the NBC and south tropical Atlantic. Their record extended back to about 85 Ka. Arz et al. (1999) undertook a more detailed analysis of the deglacial portion of the record and concluded that SST was also elevated during both the YD and H1 events. Jennerjohn and co-workers (2004) claimed that there was an asynchrony "on the order of 1000 to 2000 years between the onset of rapid millennial-scale changes and the response of the continental bio- and geospheres." We suspect instead that this asynchrony may result from the different ages of the different components of the sediment within the same sediment sample. The radiocarbon age differences of 2000 up to 6000 years that we observe between organic carbon and foraminifer carbon in the same sample is sufficient to account for the asynchrony that they observed. Weldeab and co-workers (2006) analyzed paired Mg/Ca and $\delta^{18}O$ on *Globigerinoides ruber in* the deglacial portion (only) of the record and concluded that both SST and SSS were significantly elevated

during both the YD and the H1 events. Their work thus supported and expanded the conclusions of Arz et al. (1998 and 1999). In contrast with all three of these studies, Jaeschke et al. (2007), using alkenone-derived SSTs from sediments dating back to 63 Ka, concluded that the Ti/Ca peaks coincided with lower SSTs. However, Jaeschke et al. (2007) utilized a foraminifer ^{14}C age model, while using the alkenone unsaturation index as a temperature proxy. Previous studies have shown that in regions of strong surface currents, such as the NBC, alkenone temperature reconstructions may be temporally offset from the nominal age of sedimentation given by planktonic foraminifers as a result of fine particle advection (e.g., Benthien and Müller, 2000 and Conte et al. 2006). Jaeschke et al. (2007) address the discrepancy between Mg/Ca-derived SST from Weldeab et al. (2006) and their own alkenone-derived SST in the case of the H1 event and suggest that postdepositional resuspension and transport of the alkenones could be a cause, but they did not address the potential for the same discrepancy for the entirety of their record.

In summary, published SST and SSS reconstructions of the western equatorial Atlantic are less than definitive about the direction and magnitude of change associated with NACE events and suggest that there is strong spatial heterogeneity in this oceanographically complex region. Most climate models simulating slowing of AMOC transport (whether addressing global warming or past NACE events) produce a distinctive North Atlantic-South Atlantic SST anomaly dipole with much less change of the SST in the equatorial Atlantic region (e.g., Vellinga and Wood, 2002, Zhang and

Delworth, 2005, Liu et al., 2009, Zhang et al., 2011, Menary et al., 2012 and Schmidt et al., 2012).

In the past decade, speleothem-derived precipitation records have significantly increased our knowledge of the spatial and temporal variation of late Quaternary South American paleoclimate. Most relevant to our study are high-resolution studies of speleothems from the Nordeste region. Here, Cruz et al. (2009) found negative oxygen isotopic anomalies indicating wet conditions during H1 and H2 events. They did not, however, find any significant isotopic departures during the YD. In both records of Arz et al. (1998) and our own (Fig. 3), the YD is only marked by a minor peak in Ti/Ca suggesting that little terrestrial detritus was delivered to these slope sites during the YD, but this is likely a result of near-shore sediment accumulation during higher sea levels. We observed marked increases in the Fe/K ratio that are consistent with wet conditions in the southern tropics during the YD.

In many coupled, ocean-atmosphere climate simulations (e.g., Zhang and Delworth, 2005, Broccoli et al., 2006, Stouffer et al. 2006, Timmermann et al. 2007 and Liu et al., 2009) and limited observational data (e.g., Zhang et al., 2011), NBC transport has been related to the magnitude of AMOC transport, SST variability of the North Atlantic, migration of the ITCZ, and climate of the adjacent continents. In observational studies, some mentioned previously, it has been well established that North Atlantic climate has a large impact on South American climate and paleoclimate on a variety of timescales.

The SYNTRACE study (for details, see Liu et al., 2009) was the first in which a state-of-the-art coupled climate model (National Center for Atmospheric Research

Community Climate System Model version 3, NCAR CCSM3) was run in a transient mode from the Last Glacial Maximum to present with realistic forcings, including prescribed freshwater forcing pulses during the deglaciation. In this simulation, variations in NBC northward transport (defined in Fig. 9) are tightly coupled to variations in basin-wide North Atlantic SST and variations in AMOC transport (Fig.10). This finding aligns with the results from ocean modeling (Fratantoni et al., 2000) that demand a continuity response of NBC through-flow to satisfy AMOC variation. Because the ITCZ migrates meridionally toward the hemisphere with higher SST, precipitation anomalies in the ITCZ-controlled Nordeste (Fig. 11) are expected to be positive (negative) during North Atlantic cold (warm) periods. This behavior is exactly the response observed in the SYNTRACE simulation (Fig. 12).

In some modeling experiments, when AMOC is weakened below a threshold, the NBC weakens or even reverses (e.g., Chang et al., 2006 and Wen et al., 2009 and 2011). This raises the question whether such a reversal could result in transport of sediment with Amazon provenance southeastward (instead of northwestward) along the Nordeste margin. This might be expected during NACE events if those events were accompanied by AMOC shutdown (e.g., McManus et al., 2004). We have made some effort to test this possibility for the detrital-rich intervals in CDH 86, but thus far no provenance indicators that we have measured (elemental chemistry, strontium isotopic ratios, and mineralogy of glacial sediments from both the Amazon Fan and this site) disprove a Nordeste source.

6. CONCLUSIONS

The late Quaternary paleoclimate history of tropical South America is coming into ever finer focus with the publication of many new detailed continental and marine records. One of the most robust features to emerge from many of these records is the important and, in some cases, dominant role of tropical Atlantic forcing of centennial-millennial climate variation of the adjacent continent, including the tropical Andes, the Amazon, as well as the Nordeste. The coincidence of major widespread changes in precipitation-related proxies throughout the region with NACE events, particularly Heinrich events, makes it almost an inescapable conclusion that the latter were closely linked to the former and shared a common cause. This points to very large-scale and long-lived ocean-atmosphere reorganizations. We believe that the nature of this reorganization involved major changes in AMOC and cross-equatorial NBC heat transport. However, much remains unknown about the mechanism of change (e.g., Seager and Battisti, 2007). Similar reorganizations may apply to modern and future climate, albeit with lower amplitude and on shorter (intra-annual to multi-decadal) time-scales.

7. ACKNOWLEDGEMENTS

We thank the officers, crew, and support personnel of the R/V Knorr and WHOI. We especially acknowledge the long-core coring team. The innovative design work, tireless deck work, and leadership, of James Broda were indispensable. The work was made possible by the cooperation of the Brazilian navy and the government of Brazil. We thank one anonymous reviewer and David Lea who spent an enormous amount of time to provide us with a very detailed and helpful review. Phil Meyers also helped greatly in the review and editorial process. Funding for the cruise and post-cruise science was

provided to PAB by NSF-OCE-0823650.

8. REFERENCES

Anand, P., Elderfield, H., Conte, M. H., 2003. Calibration of Mg/Ca thermometry in planktonic foraminifera from a sediment trap time series. Paleoceanography 18(2), 1050, doi: 10.1029/2002PA000846.

Antonov, J. I., Seidov, D., Boyer, T. P., Locarnini, R. A., Mishonov, A. V., Garcia, H. E., Baranova, O. K., Zweng, M. M., Johnson, D. R., 2010. World Ocean Atlas 2009, Volume 2: Salinity. S. Levitus, Ed. NOAA Atlas NESDIS 69, U.S. Government Printing Office, Washington, D.C., 184 pp.

Arbuszewski, J., deMenocal, P., Kaplan, A., Farmer, E.C., 2010. On the fidelity of shell-derived delta O-18(seawater) estimates. Earth and Planetary Sciences Letters 300, 185–196.

Arz, H. W., Patzold, J., Wefer, G., 1998. Correlated millennial-scale changes in surface hydrography and terrigenous sediment yield inferred from last-glacial marine deposits off northeastern Brazil. Quaternary Research 50, 157 – 166.

Arz, H. W., Patzold, J., Wefer, G., 1999. The deglacial history of the western tropical Atlantic as inferred from high-resolution stable isotope records off northeastern Brazil, Earth and Planetary Sciences Letters 167, 105–117.

Baker, P.A., Seltzer, G.O., Fritz, S.C., Dunbar, R.B., Grove, M.J., Tapia, P.M., Cross, S.L., Rowe, H.D., Broda, J.P., 2001a. The history of South American tropical precipitation for the past 25,000 years. Science 291, 640–643.

Baker, P.A., Rigsby, C.A., Seltzer, G.O., Fritz, S.C., Lowenstein, T.K., Bacher, N.P., Veliz, C., 2001b. Tropical climate changes at millennial and orbital timescales on the Bolivian Altiplano. Nature 409, 698–700.

Bard, E., 1988. Correction of accelerator mass spectrometry ^{14}C ages measured in planktonic foraminiferas: Paleoceanographic implications. Paleoceanography 3, 635–645.

Barker, S., Greaves, M., Elderfield, H., 2003. A study of cleaning procedures used for foraminiferal Mg/Ca paleothermometry. Geochemistry Geophysics Geosystems 4, 8407, doi:10.1029/2003GC000559.

Bemis, B.E., Spero, H.J., Bijma, J., Lea, D.W., 1998. Reevaluation of the oxygen isotopic composition of planktonic foraminifera: Experimental results and revised paleotemperature equations. Paleoceanography 13, 150–160.

Benthien, A., Müller, P. J., 2000. Anomalously low alkenone temperatures caused by lateral particle and sediment transport in the Malvinas Current region, western Argentine Basin. Deep Sea Research, Part I 47, 2369–2393.

Bigarella, J. J., Mabesoone, J.M., Caldas Lins, C.J., Mota, F.O., 1965. Paleogeographical features of the Sierra Grande and Pimenteira Formations (Parnaíba Basin, Brazil). Palaeogeography, Palaeoclimatology, Palaeoecology 1, 259-296.

Bintanja, R., van de Wal, R.S.W., Oerlemans, J., 2005. Modelled atmospheric temperatures and global sea levels over the past million years. Nature 437, 125-128.
Bond, G. C., Lotti, R., 1995. Iceberg discharges into the North Atlantic on millennial time scale during the Last Glaciation. Science 267, 1005–1010.

Broccoli, A.J., Dahl, K.A., Stouffer, R.J., 2006. Response of the ITCZ to Northern Hemisphere cooling. Geophysical Research Letters 33, L01702, doi:10.1029/2005GL024546.

Chang, P., Ji, L., Li, H., 1997. A decadal climate variation in the tropical Atlantic Ocean from thermodynamic air–sea interactions. Nature 385, 516 –518.

Chang, P., Zhang, R., Hazeleger, W., Wen, C., Wan, X., Ji, L., Haarsma, R., Breugem, W. P., Seidel, H., 2008. An oceanic bridge between abrupt changes in North Atlantic climate and the African monsoon. Nature Geosciences 1, 444–448, doi:10.1038/ngeo218.

Cheng, H., Sinha, A., Cruz, F.W., Wang, X., Edwards, R.L., d'Horta, F.M., Ribas, C.C., Vuille, M., Stott, L.D., Auler, A.S., 2013. Climate change patterns in Amazonia and biodiversity. Nature Communications, doi: 10.1038/ncomms2415.

Chiang, J.C.H., Kushnir, Y., Giannini, A., 2002. Deconstructing Atlantic Intertropical Convergence Zone variability: influence of the local cross-equatorial sea surface temperature gradient and remote forcing from the eastern equatorial Pacific. Journal of Geophysical Research 107 (D1), 4004. doi:10.1029/2000/JD000307.

Chiang, J.C.H., Biasutti, M., Battisti, D.S., 2003. Sensitivity of the Atlantic Intertropical Convergence Zone to Last Glacial Maximum boundary conditions. Paleoceanography 18 (4) 1094, doi:10.1029/2003PA000916.

Conte, M. H., Sicre, M.A. Ruhlemann, C. Weber, J. C. Schulte, S. Schulz-Bull, D. Blanz, T., 2006. Global temperature calibration of the alkenone unsaturation index (UK37) in surface waters and comparison with surface sediments. Geochemistry Geophysics Geosystems 7, Q02005, doi:10.1029/2005GC001054.

Cruz, F.W., Vuille, M., Burns, S.J., Wang, X.F., Cheng, H., Werner, M., Edwards, R.L., Karmann, I., Auler, A.S., Nguyen, H., 2009. Orbitally driven east–west antiphasing of South American precipitation. Nature Geosciences 2, 210–214.

Dansgaard, W., Johnsen, S.J., Clausen, H. B., Dahl-Jensen, D., Gundestrup, N. S., Hammer, C. U., Hvidberg, C. S., Steffensen, J. P., Sveinbjörnsdottir, A. E., Jouzel, J., Bond, G., 1993. Evidence for general instability of past climate from a 250-kyr ice-core record. Nature 364, 218–220.

Dwyer, G.S., Cronin, T.M., Baker, P.A., Raymo, M.E., Buzas, J.S., Correge, T. 1995. North Atlantic deepwater temperature change during Late Pliocene and Late Quaternary climatic cycles. Science 270, 1347-1351.

Eglinton T. I., Benitez-Nelson B. C., Pearson A., McNichol A. P., Bauer J. E., Druffel E. R. M., 1997. Variability in radiocarbon ages of individual organic compounds from marine sediments. Science 277, 796–799.

Fairbanks R.G., Mortlock R.A., Chiu T.-C., C. L., Kaplan A., Guilderson T.P., Fairbanks T.W., Bloom A.L., Grootes P.M., Nadeau M.-J., 2005. Radiocarbon calibration curve spanning 0 to 50,000 years BP based on paired $^{230}Th/^{234}U/^{238}U$ and ^{14}C dates on pristine corals. Quaternary Science Reviews 24, 1781–1796.

Ferguson, J. E., Henderson, G. M., Kucera, M., Rickaby, R. E. M., 2008. Systematic change of foraminiferal Mg/Ca ratios across a strong salinity gradient, Earth and Planetary

Sciences Letters 265, 153–166.

Fratantoni, D.M., Johns, W.E., Townsend, T.L., Hurlburt, H.E., 2000. Low-latitude circulation and mass transport pathways in a model of the Tropical Atlantic Ocean. Journal of Physical Oceanography 30, 1944–1966.

Fritz, S.C., Baker, P.A. Ekdahl, E. Seltzer, G.O. Stevens, L.R., 2010. Millennial-scale climate variability during the last glacial period in the tropical Andes. Quaternary Science Reviews 29, 1017-1024.

Grootes, P.M., Stuiver, M., White, J.W.C., Johnsen, S.J., Jouzel, J., 1993. Comparison of oxygen isotope records from the GISP2 and GRIP Greenland ice cores. Nature 366, 552-554.

Hastenrath, S., 1991. Climate Dynamics of the Tropics. Kluwer Academic Publishers, Dordrecht, Netherlands.

Hastenrath, S., Greischar, L., 1993. Circulation mechanisms related to northeast Brazil rainfall anomalies. Journal of Geophysical Research 98, 5093-5102.

Hastenrath, S., Heller, L., 1977. Dynamics of climatic hazards in Northeast Brazil. Quarterly Journal of the Royal Meterological Society 103, 77-92.

Heinrich, H., 1988. Origin and consequences of cyclic ice rafting in the northeast Atlantic Ocean during the past 130,000 years. Quaternary Research 29, 142–152.

Hemming, S. R., 2004. Heinrich events: Massive late Pleistocene detritus layers of the North Atlantic and their global climate imprint. Reviews of Geophysics 42, RG1005, doi:10.1029/ 2003RG000128.

Hodell, D.A., Anselmetti, F.S., Ariztegui, D., Brenner, M., Curtis, J.H., Gilli, A., Grzesik, D.A., Guilderson, T.J., Muller, A.D., Bush, M.B., Correa-Metrio, Y.A., Escobar, J., Kutterolf, S., 2008. An 85-ka Record of Climate Change in Lowland Central America. Quaternary Science Reviews 27, 1152- 1165.

Honisch, B., Allen, K. A., Lea, D. W., Spero, H. J., Eggins, S. M., Arbuszewski, J., deMenocal, P., Rosenthal, Y., Russell, A.D., Elderfield., H., 2013. The influence of salinity on Mg/Ca in planktic foraminifers: Evidence from cultures, core-top sediments and

complementary $\delta^{18}O$. Geochimica et Cosmochimica Acta 121, 196-213.

Jaeschke, A., Ruhlemann, C., Arz, H., Heil, G., Lohmann, G., 2007. Coupling of millennial-scale changes in sea surface temperature and precipitation off northeastern Brazil with high-latitude climate shifts during the last glacial period. Paleoceanography 22, PA4206.

Jennerjahn, T. C., Ittekkot, V., Arz, H.W., Behling, H., Pätzold, J., Wefer, G., 2004. Asynchronous terrestrial and marine signals of climate change during Heinrich events. Science 306, 2236–2239.Johns, W.E., Lee, T.N., Beardsley, R., Candela, J., Castro, B., 1998. Annual cycle and variability of the North Brazil Current. Journal of Physical Oceanography 28, 103–128.

Kanner, L.C., Burns, S.J. Cheng, H. Edwards, R.L., 2012. High-latitude forcing of the South American Summer Monsoon during the last Glacial. Science 335, 570-573.

Kısakürek, B., Eisenhauer, A., Böhm, F., Garbe-Schönberg, D., Erez, J., 2008. Controls on shell Mg/Ca and Sr/Ca in cultured planktonic foraminiferan, *Globigerinoides ruber* (white). Earth and Planetary Sciences Letters 273, 260–269.

Lea D.W., Pak D.K., Spero, H. J., 2000. Climate impact of late Quaternary equatorial Pacific sea surface temperature variations. Science 289, 1719–1724.

Lewis, S.L., Brando, P.M., Phillips, O.L., van der Heijden, G.M.F., Nepstad, D., 2011. The 2010 Amazon drought. Science 331, 554.

Lisiecki, L.E., Raymo, M.E., 2005. A Pliocene-Pleistocene stack of 57 globally distributed benthic $\delta^{18}O$ records, Paleoceanography 20, PA1003, doi:10.1029/2004PA001071. Liu, Z., Otto-Bliesner, B., He, F., Brady, E., Clark, P., Lynch-Steiglitz, J., Carlson, A., Curry, W., Brook, E., Jacob, R., Erikson, D., Kutzbach, J., Cheng, J., 2009. Transient simulation of deglacial Climate Evolution with a new mechanism for Bolling-Allerod warming. Science 325, 310-314.

Locarnini, R. A., Mishonov, A. V., Antonov, J. I., Boyer, T. P., Garcia, H. E., Baranova, O. K., Zweng, M. M., Johnson, D. R., 2010. World Ocean Atlas 2009, Volume 1: Temperature. S. Levitus, Ed. NOAA Atlas NESDIS 68, U.S. Government Printing Office, Washington, D.C.

Maher, B.A., Thompson, R., 1995. Paleorainfall reconstructions from pedogenic magnetic susceptibility variations in the Chinese loess and paleosols. Quaternary

Research 44, 383–391.

Marengo, J.A., Nobre, C., Tomasella, J., Oyama, M.D., DeOlivera, G.S., 2008. The drought of Amazonia in 2005. Journal of Climate 21, 495-516.

Marques, M., Costa, M. F., Mayorga, M. I. O., Pinheiro, P., 2004. The water environment: anthropogenic pressures and ecosystem changes in the Atlantic drainage basins of Brazil. AMBIO 33, 68–77.

McManus, J. F., Francois, R., Gherardi, .J.M., Keigwin, L. D., Brown-Leger, S., 2004. Collapse and rapid resumption of Atlantic meridional circulation linked to deglacial climate changes. Nature 428, 834–837.

Menary, M.B., Park, W., Lohmann, K., Vellinga, M., Palmer, M.D., Latif, M., Junclaus, J.H., 2012. A multimodel comparison of centennial Atlantic meridional overturning circulation variability. Climate Dynamics 38, 2377–2388.

Mulitza, S., Prange, M., Stuut, J.-B., Zabel, M., von Dobeneck, T., Itambi, A.C., Nizou, J., Schulz, M., Wefer G., 2008. Sahel megadroughts triggered by glacial slowdowns of Atlantic meridional overturning. Paleoceanography 23, PA4206, doi:10.1029/2008PA001637.

NGRIP, 2004. High-resolution record of Northern Hemisphere climate extending into the last interglacial period. Nature 431, 147-151.

Nobre, P., Shukla, J., 1996. Variations of sea surface temperature, wind stress, and rainfall over the tropical Atlantic and South America. Journal of Climate 9, 2464–2479.

Nürnberg, D., Bijma, J. , Hemleben, C., 1996. Assessing the reliability of magnesium in foraminiferal calcite as a proxy for water mass temperatures. Geochimica et Cosmochimica Acta 60, 803–814.

Obrochta, S.P., Miyahara, H., Yokoyama, Y., and Crowley, T.J., 2012. A re-examination of evidence for the North Atlantic "1500-year cycle" at Site 609. Quaternary Science Reviews 55, 23–33.

Obrochta, S.P., Yokoyama, Y., Morén, J., Crowley, T.J., 2014. Conversion of GISP2-based sediment core age models to the GICC05 extended chronology. Quaternary Geochronology 20, 1-7.

Otto-Bliesner, B.L., Brady, E.C., 2010. The sensitivity of the climate response to the

magnitude and location of freshwater forcing: Last glacial maximum experiments. Quaternary Science Reviews 29, 56–73.

Peterson, L.C., Haug, G.H., 2006. Variability in the mean latitude of the Atlantic Intertropical Convergence Zone as recorded by riverine input of sediments to the Cariaco Basin (Venezuela). Palaeogeography, Palaeoclimatology, Palaeoecology 234, 97-113.

Richardson, P.L., Hufford, G. E., Limeburner, R., Brown, W. S., 1994. North Brazil Current retroflection eddies. Journal of Geophysical Research 99, 5081–5093.

Ruhlemann, C., Frank, M., Hale, W., Mangini, A., Mulitza, S., Muller, P. J., Wefer, G., 1996. Late Quaternary productivity changes in the western equatorial Atlantic: Evidence from ^{230}Th-normalized carbonate and organic carbon accumulation. Marine Geology 135, 127–152.

Sachs, J.P., Anderson, R.F., Lehman, S.J., 2001. Glacial surface temperature of the Southeast Atlantic Ocean. Science 293, 2077– 2079.

Schmidt, M.W., Chang, P., Hertzberg, J.E., Them II, T.R., Ji, L., Otto-Bliesner, B.L., 2012. Impact of abrupt deglacial climate change on tropical Atlantic subsurface temperatures. Proceedings National Academy of Sciences USA 109, 14348-14352.

Schott, F., Stramma, L., Fischer, J., 1995. The warm water inflow into the western tropical Atlantic boundary regime, spring 1994. Journal of Geophysical Research 100, 24745–24760.

Seager, R., Battisti, D.S., 2007. Challenges to our understanding of the general circulation: abrupt climate change. In: Schneider, T. and Sobel, A.H. (Ed.), The Global Circulation of the Atmosphere. Princeton University Press, 331-371.

Stramma, L., Fischer, J., Reppin, J., 1995. The North Brazil Undercurrent. Deep Sea Research, Part I 42, 773–795.

Stuut, J.-B., Zabel, M., Ratmeyer, V., Helmke, P., Schefur, E., Lavik, G., Schneider, R., 2005. Provenance of present-day eolian dust collected off NW Africa. Journal of Geophysical Research 110, D04202, doi: 10.1029/2004JD005161.

Svensson, A., Andersen, K. K., Bigler, M., Clausen, H. B., Dahl-Jensen, D., Davies, S. M., Johnsen, S. J., Muscheler, R., Parrenin, F., Rasmussen, S. O., Röthlisberger, R., Seierstad, I., Steffensen, J. P., Vinther, B. M., 2008. A 60,000 year Greenland stratigraphic ice core chronology. Climates of the Past 4, 47–57.

Talley, L., Pickard, G., Emery, W., Swift, J., 2011. Descriptive Physical Oceanography: An Introduction, Elsevier Academic.

Thunell, R., Tappa, E., Pride, C., Kincaid, E., 1999. Sea-surface temperature anomalies associated with the 1997–1998 El Nino recorded in the oxygen isotope composition of planktonic foraminifera. Geology 27, 843–846.

Timmermann A., Okumura Y., An S.-I., Clement A., Dong B., Guilyardi E., Hu A., Jungclaus J., Krebs U., Renold M., Stocker T.F., Stouffer R.J., Sutton R., Xie S.-P., Yin J., 2007. The influence of a weakening of the Atlantic meridional overturning circulation on ENSO. Journal of Climate 20, 4899–4919.

Vellinga, M., Wood, R.A., 2002. Global climatic impacts of a collapse of the Atlantic thermohaline circulation. Climatic Change 54, 251–267.

Vellinga, M., Wu, P., 2004. Low-latitude freshwater influence on centennial variability of the Atlantic thermohaline circulation. Journal of Climate 17, 4498–4511.

Volkoff, B., 1983. Iron constituents of the latosolic cover in northeast Brazil. In: A.J. Melfi and A. Carvalho (Editors), Lateritization Processes, University of Sao Paulo Press, Sao Paulo, pp. 527-540.

Wang, X., Auler, A. S., Edwards, R. L., Cheng, H., Cristalli, P. S., Smart, P. L., Richards, D. A., Shen, C.-C., 2004. Wet periods in northeastern Brazil over the past 210 kyr linked to distant climate anomalies. Nature 432, 740-743.

Wang, X. F., Auler, A.S., Edwards, R.L., Cheng, H., Ito, E., Dorale, J., 2014. Rapid Amazonian moisture oscillations correlated with Dansgaard–Oeschger cycles, in preparation.

Ward, N.M., Folland, C.K., 1991. Prediction of seasonal rainfall in the north Nordeste of Brazil using eigenvectors of sea-surface temperatures. International Journal of Climatology 11, 711–743.

Weaver, C.E., 1976. The nature of TiO_2 in kaolinite. Clays and Clay Minerals 24, 215–218.

Wen, C., Chang, P., Saravanan, R., 2010. Effect of Atlantic meridional overturning circulation changes on tropical Atlantic sea surface temperature variability: A 2½-layer reduced-gravity ocean model study. Journal of Climate 23, 312–332.

Wen, C., Chang, P., Saravanan, R., 2011. Effect of Atlantic Meridional Overturning Circulation on Tropical Atlantic Variability: A Regional Coupled Model Study. Journal of Climate 24, 3323–3343.

Weldeab, S., Schneider, R. R., Kolling, M., 2006. Deglacial sea surface temperature and salinity increase in the western tropical Atlantic in synchrony with high latitude climate in- stabilities. Earth and Planetary Sciences Letters 241, 699– 706.

Zhang, R., Delworth, T.L., 2005. Simulated Tropical Response to a Substantial Weakening of the Atlantic Thermohaline Circulation. Journal of Climate 18, 1853-1860.

Zhang, D., Msadek, R., McPhaden, M. J., Delworth, T., 2011. Multidecadal variability of the North Brazil Current and its connection to the Atlantic meridional overturning circulation. Journal of Geophysical Research 116, C04012, doi: 10.1029/2010JC006812.

Figure 1. SRTM image of northern South America with regional inset image (Google Earth) showing location of cores CDH-86 (this study) and GeoB 3912-1 (Arz et al., 1998) relative to the present-day mouths of the Amazon and Parnaíba Rivers. During sea level lowstands of the Last Glacial, both rivers crossed the wide shelf and delivered sediment directly to the outer shelf and upper continental slope.

Figure 2. Left panel: Age model of core CDH86, foraminifera derived radiocarbon ages converted to calendar age in blue, LR04 age tie points in red. Right panel: Difference between the organic carbon and foraminifer ages, plotted against their radiocarbon age based on analysis of the foraminifers. Only midpoints of radiocarbon probability density functions are shown for simplicity.

Figure 3. Ti/Ca ratio from sediments of Core CDH 86 (black line) and weight percent detrital carbonate from North Atlantic core ODP Site 609 (gray line)(data from Obrochta et al., 2012). The latter is considered to be an accurately dated record of Heinrich events. From 70 Ka to present, every Ti/Ca peak in CDH 86 has a correlative Heinrich event of the same age within dating uncertainties of both records. H2, ca. 25 Ka, is not represented by a Ti/Ca peak in CDH 86, although it is clearly present farther south (Arz et al., 1998). The largest Ti/Ca peak in the entire CDH 86 record is ca. 110 Ka and has no northern counterpart.

Figure 4. Ti/Ca and Fe/K time series for CDH 86. Almost every Ti/Ca peak has a Fe/K counterpart. However, some Fe/K maxima have no Ti/Ca counterpart. Moreover, the Fe/K peaks tend to be somewhat longer duration, perhaps indicating that climate over the continent became wet and remained wet longer (or weathered soil products remained on the surface after climate had dried). Note the large Fe/K peak of Younger Dryas age despite only a small Ti/Ca peak—the latter is likely because the river mouth was much farther from the coring site during the higher sea levels of the deglacial and Holocene. Also note the changing character of both proxies between the earlier and later periods of the record.

Figure 5. Principal component analysis of XRF data from core CDH86. Components 1 and 2 respectively explain 26.1% and 23.1% of the variability. Of particular note is the different loading of three terrigenous elements, Fe, Ti, and K. These each have value as provenance indicators.

Figure 6. . Ti/Ca and magnetic susceptibility (MS) time series for CDH 86. Every Ti/Ca maximum (low and high amplitude alike) since 70 Ka and almost every maximum prior to that, is accompanied by a MS minimum. We believe that these minima result from the precipitation of iron oxides in lateritic crusts that are left behind on the landscape during tropical weathering. Again, as for Fe/K, the character of MS peaks prior to 70 Ka differs from those after 70 Ka.

Figure 7. Ti/Ca and Mg/Ca - determined sea surface temperature (SST) time series. The latter record was smoothed with a three point moving average. In most cases Ti/Ca maxima are accompanied by maxima of SST, particularly after 70 Ka. Nevertheless, this is not a particularly compelling relationship and it seems possible that: the western equatorial Atlantic is not a "sweet spot" for recording the southern half of the posited Atlantic SST meridional dipole and this near coastal, equatorial site is subject to a great deal of local surface oceanographic variability.

Figure 8. Time series of Ti/Ca and $\delta^{18}O_{swivc}$, the global ice-volume-corrected oxygen isotopic composition of seawater (itself determined as the residual of the oxygen isotopic composition of foraminiferal shell carbonate and temperature fractionation determined from Mg/Ca – SST). $\delta^{18}O_{swivc}$, as a residual of two determination that are themselves rather noisy, was smoothed by a 5-point moving average. $\delta^{18}O_{swivc}$, is believed to be a proxy for local sea-surface salinity (SSS). In all save one case (ca. 60 Ka), Ti/Ca maxima are accompanied by minima of $\delta^{18}O_{swivc}$. Taken at face value, a typical $\delta^{18}O_{swivc}$ minimum in the record of 0.5‰ could be produced by 1/8 dilution of seawater by river water with a $\delta^{18}O$ of -4‰ yielding seawater with a salinity lowered from 36 to 32 psu (a salinity typical of the modern Amazon plume about 1000 km from the mouth of the river).

Figure 9. North Brazil Current (NBC) northward transport (cm s^{-1}) calculated from the CCSM3 SYNTRACE model for the late Holocene, pre-industrial era between 2 and 1 Ka. Longitude-depth section of meridional velocity averaged over 8°S to 4°S. NBC transport is defined as the northward integrated volume transport within the highlighted box. This transport resembles that of the observational record in both flux and location.

Figure 10. AMOC (blue line) and NBC (red line) transport (Sverdrups) and the AMO Index (green line, °C) for the full SYNTRACE simulation from 22 Ka to modern (pre-industrial). NBC transport is integrated within (40°W to 30°W, 8°S to 4°S, 0 to 400 m water depth. AMOC transport is defined as the maximum transport within (20°N to 70°N, 0.5 to 5 km water depth). AMO is the area-weighted North Atlantic (0° to 70°N, 90°W to 40°E) SST, with global trends and influence of sea ice removed.

Figure 11. Climatology (pre-industrial era) of the precipitation (mm/day) and 850 hPa winds (unit length is 10 m/s) over South America in TraCE21 (CCSM 3.0). Annual precipitation (upper panel) and DJF precipitation (lower panel). Wet season moisture source for the Nordeste is the adjacent southern equatorial Atlantic; its SST is expected to correlate with moisture advective flux and precipitation on land.

Figure 12. Annual mean precipitation in the Nordeste of Brazil (50°W to 35°W, 15°S to 0°S) for the full SYNTRACE simulation from 22 Ka to modern (pre-industrial). Prominent maxima in precipitation over the Nordeste are simulated for all North Atlantic cold events, including H1, YD, and the Holocene 8.2 Ka event.

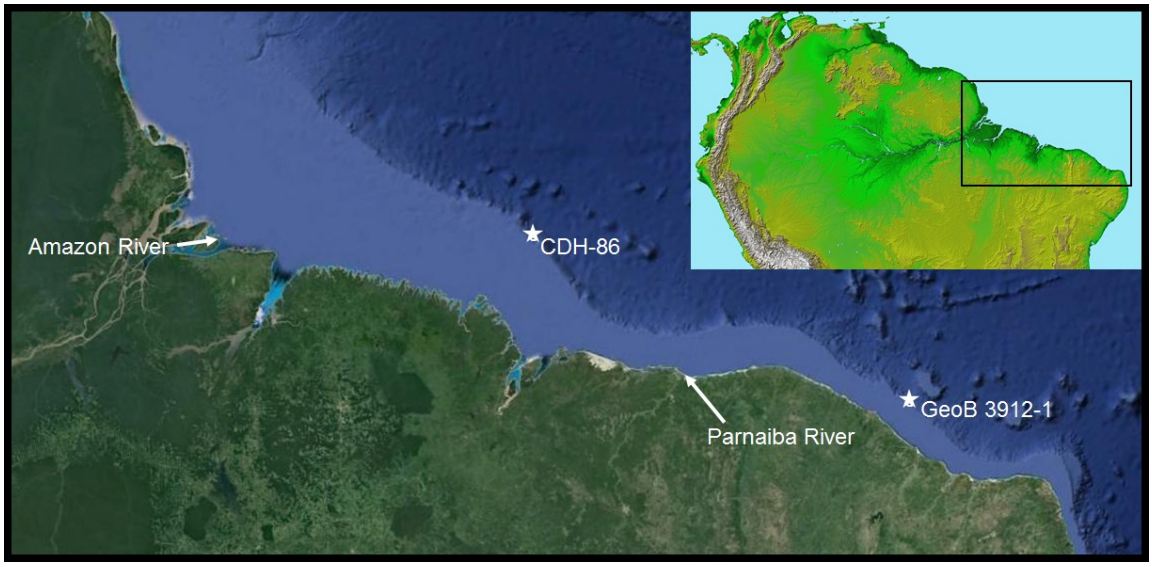

Figure 1

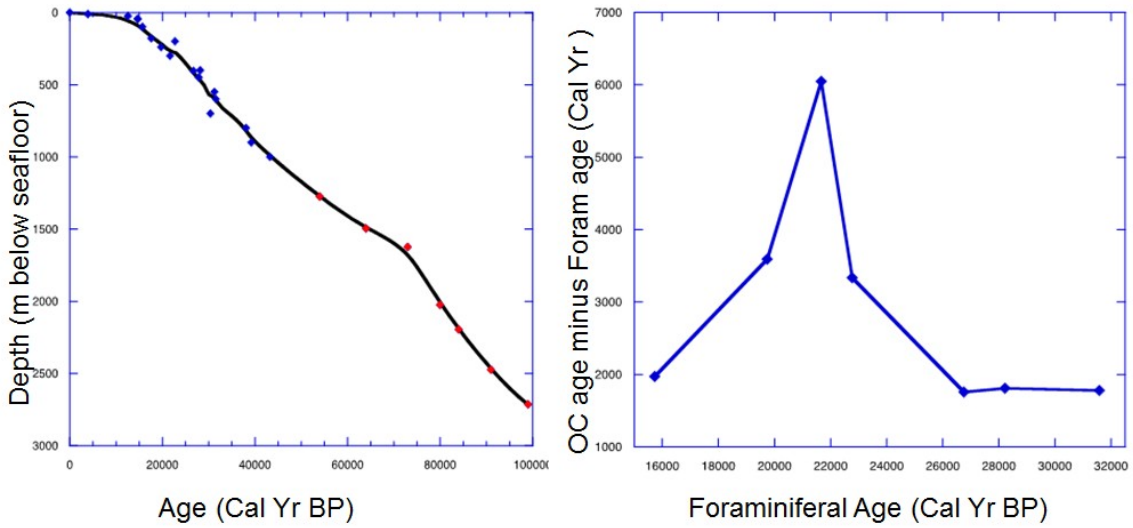
Depth (m below seafloor)
0
500
1000
1500
2000
2500
3000
0
20000
40000
60000
80000
Age (Cal Yr BP)
OC age minus Foram age (Cal Yr)
7000
6000
5000
4000
3000
2000
1000
16000
18000
20000
22000
24000
26000
28000
30000
32000
Foraminiferal Age (Cal Yr BP)

Figure 2

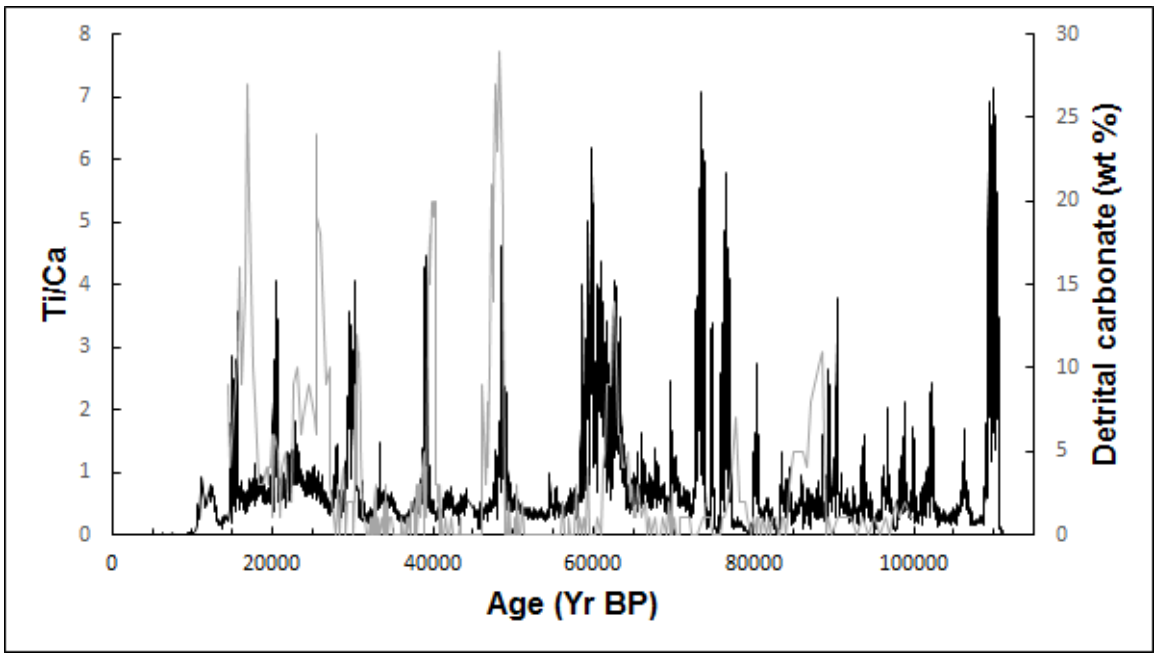
Ti/Ca
Detrital carbonate (wt %)
Age (Yr BP)
0
1
2
3
4
5
6
7
8
0
5
10
15
20
25
30
0
20000
40000
60000
80000
100000

Figure 3

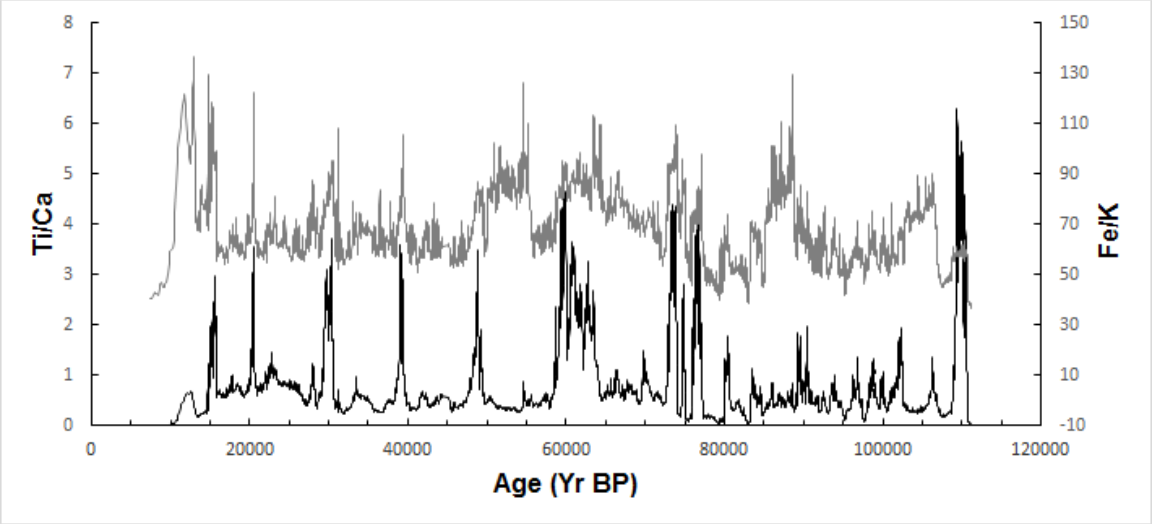
Ti/Ca
Fe/K
Age (Yr BP)
0
1
2
3
4
5
6
7
8
-10
10
30
50
70
90
110
130
150
0
20000
40000
60000
80000
100000
120000

Figure 4

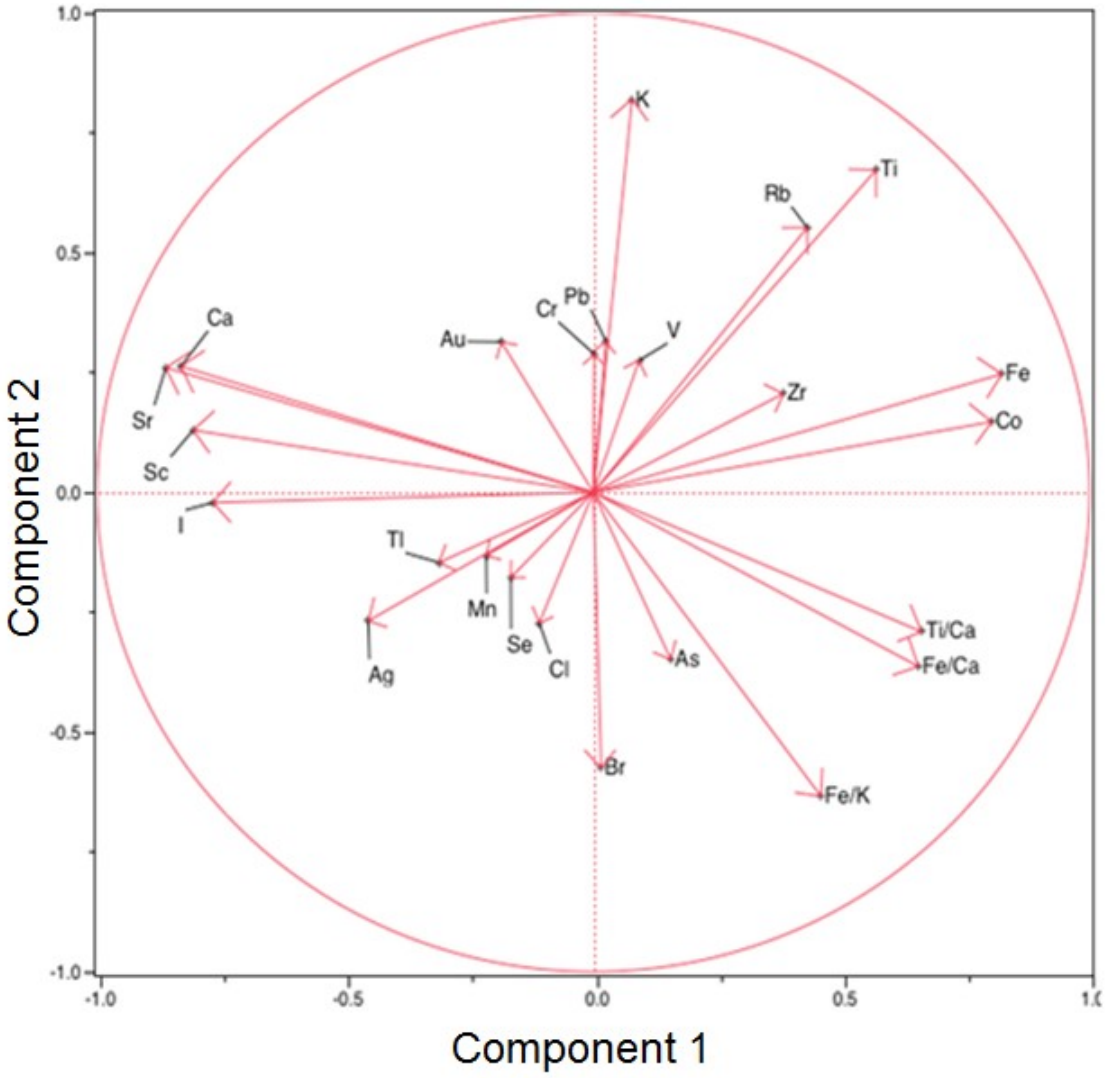
Component 2
Component 1
1.0
0.5
0.0
-0.5
-1.0
K
Ti
Rb
Ca
Cr
Pb
Au
V
Fe
Zr
Co
Sr
Sc
I
Tl
Mn
Se
Cl
Ag
As
Ti/Ca
Fe/Ca
Br
Fe/K

Figure 5

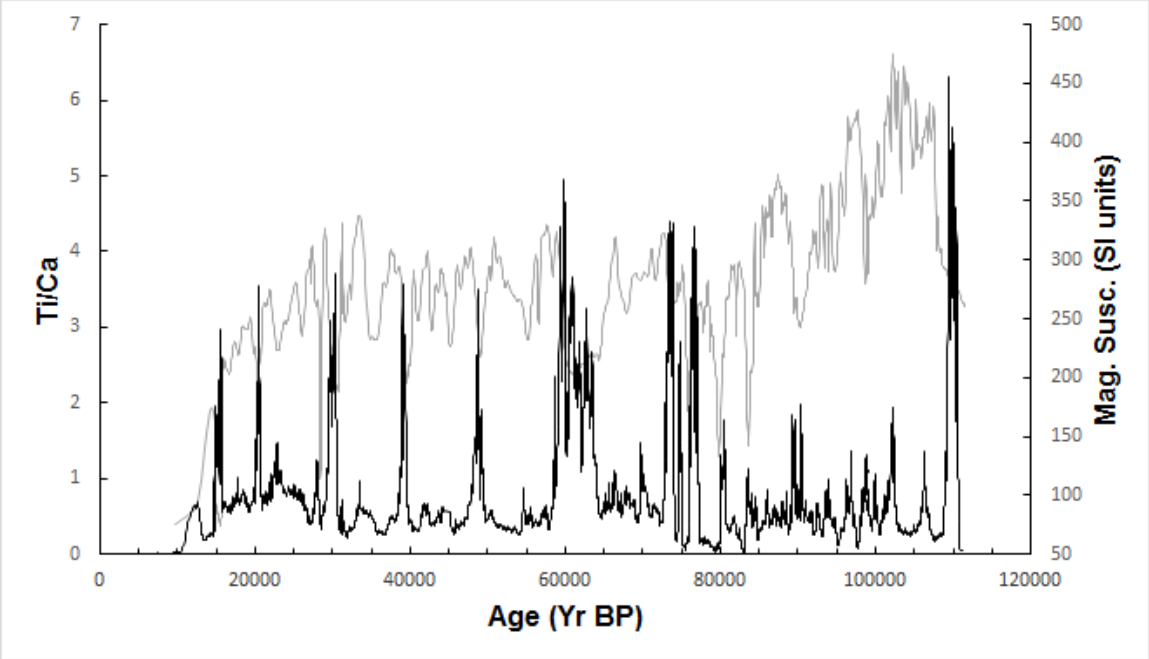
Ti/Ca
Mag. Susc. (SI units)
Age (Yr BP)
0
1
2
3
4
5
6
7
50
100
150
200
250
300
350
400
450
500
0
20000
40000
60000
80000
100000
120000

Figure 6

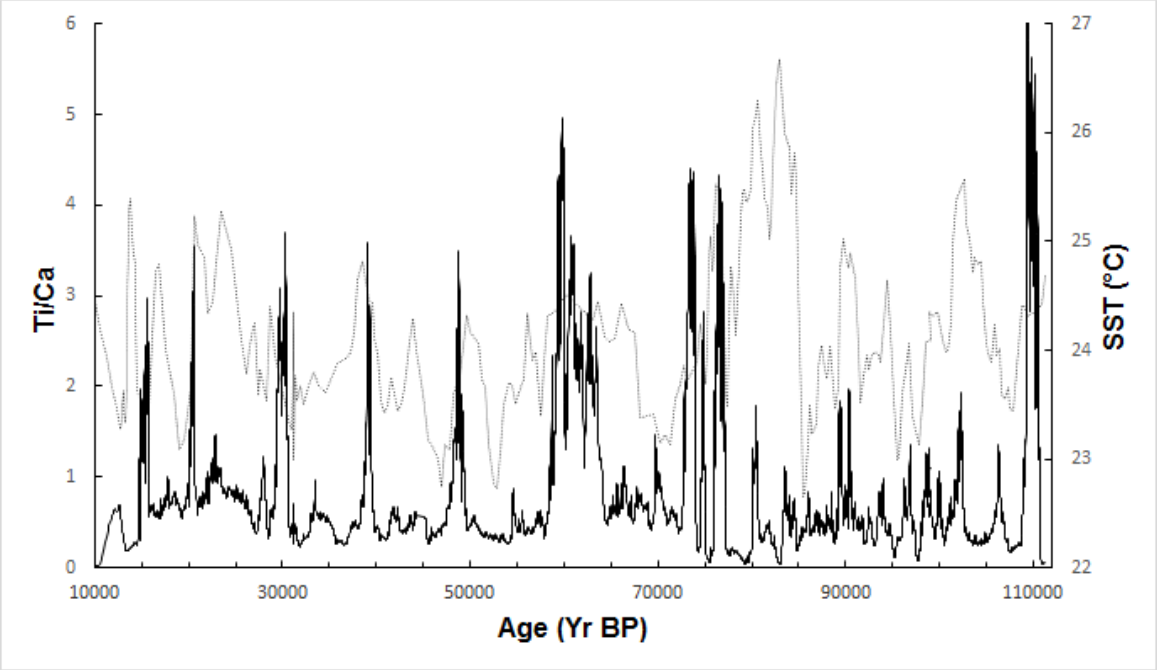
Ti/Ca
SST (°C)
Age (Yr BP)
0
1
2
3
4
5
6
22
23
24
25
26
27
10000
30000
50000
70000
90000
110000

Figure 7

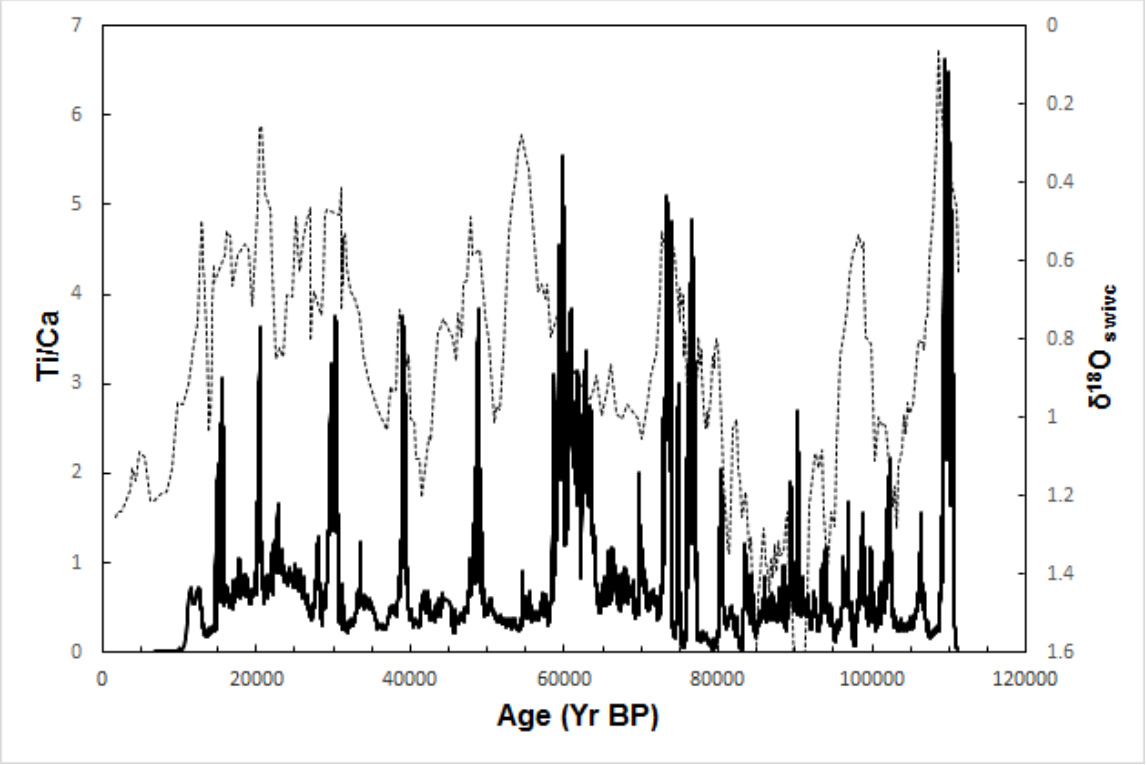
Ti/Ca
δ18O swivc
Age (Yr BP)
0
1
2
3
4
5
6
7
0.2
0.4
0.6
0.8
1
1.2
1.4
1.6
0
20000
40000
60000
80000
100000
120000

Figure 8

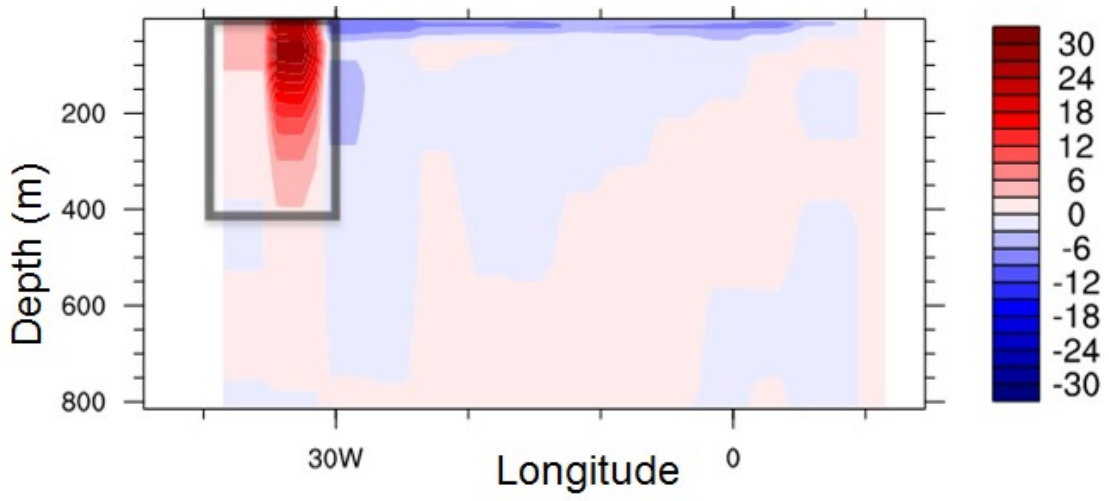
Depth (m)
200
400
600
800
30W
Longitude
0
30
24
18
12
6
0
-6
-12
-18
-24
-30

Figure 9

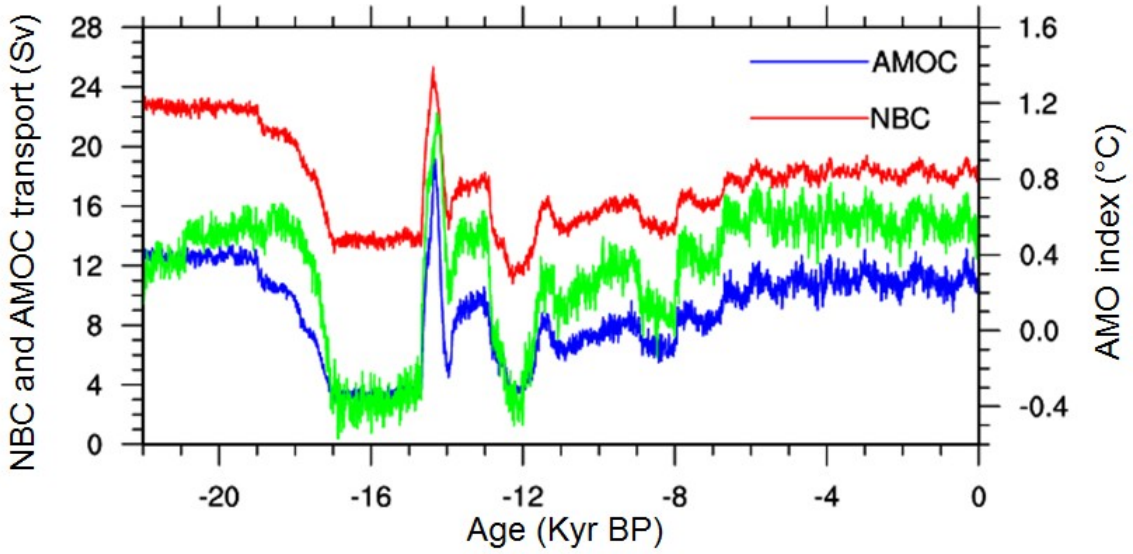
NBC and AMOC transport (Sv)
28
24
20
16
12
8
4
0
1.6
1.2
0.8
0.4
0.0
-0.4
AMO index (°C)
AMOC
NBC
-20
-16
-12
-8
-4
0
Age (Kyr BP)

Figure 10

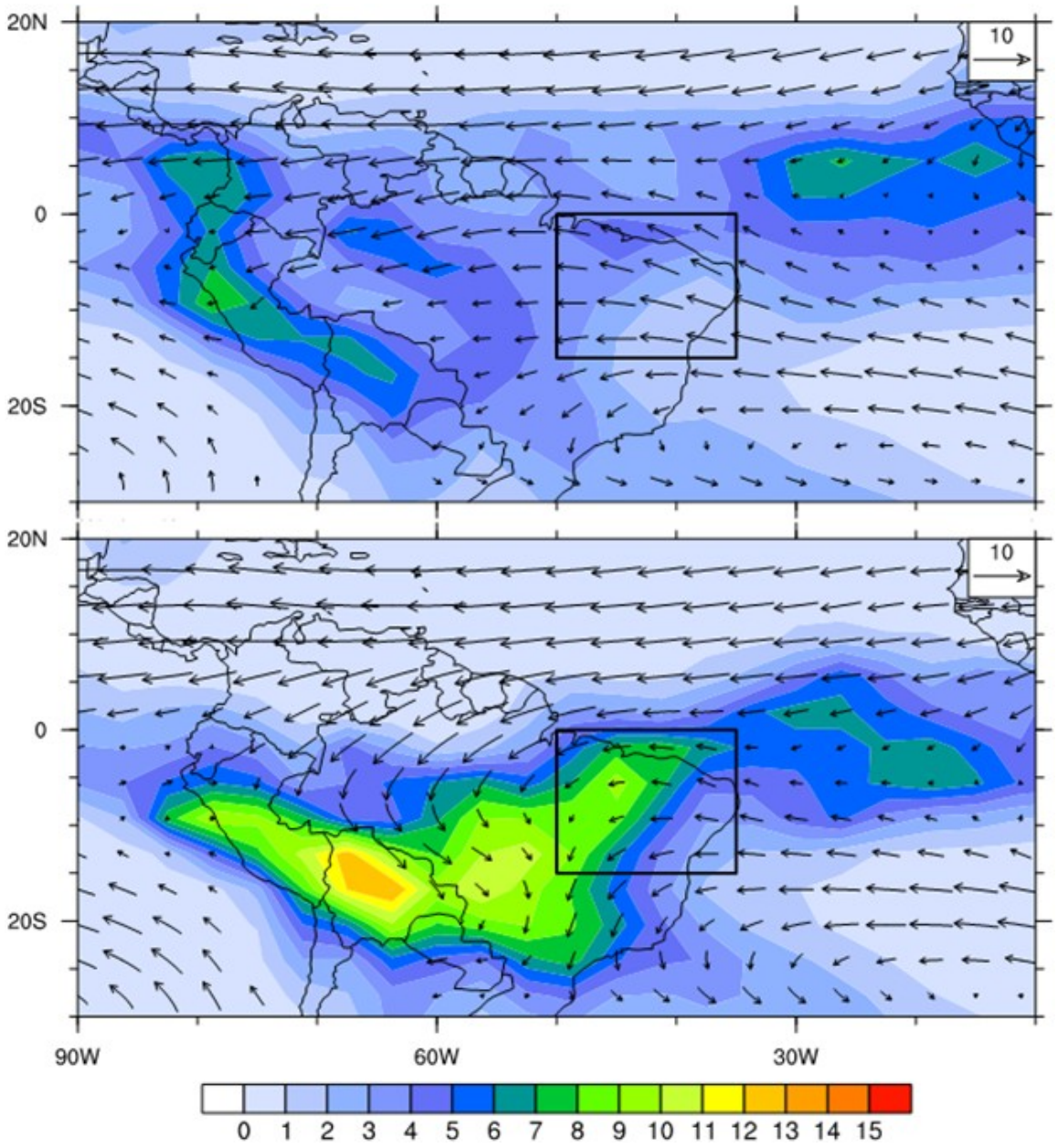

Figure 11

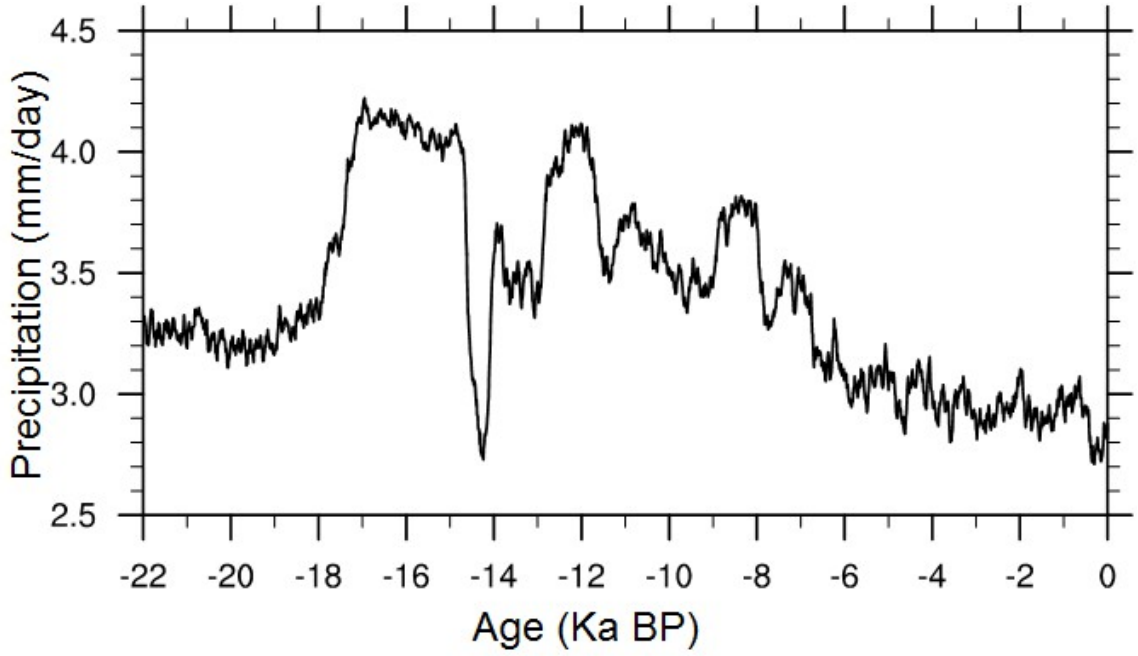
Precipitation (mm/day)
4.5
4.0
3.5
3.0
2.5
-22
-20
-18
-16
-14
-12
-10
-8
-6
-4
-2
0
Age (Ka BP)

Figure 12

Table 1: Radiocarbon dates with NOSAMS receipt number, sample ID, sample type, uncorrected age and 2σ error, and calibrated age and error.

Table 1

Receipt #	Core	Depth (cm)	Type	^{14}C Age	Age Error	Calendar Age	Calendar Age Error
83905	BC82	11	Foraminifera	3890	25	4333	55
102277	GGC81	10	Foraminifera	11150	45	12998	47
83906	GGC81	30	Foraminifera	13000	50	15143	111
101326	BC82	44	Foraminifera	12900	55	15029	109
82323	GGC81	85	Foraminifera	13850	45	16130	123
83715	GGC81	85	Organic Carbon	14800	85	17702	223
82318	CDH86	100	Foraminifera	19450	85	23176	178
83309	CDH86	100	Organic Carbon	21700	120	26111	168
101327	GGC86	165	Foraminifera	14950	70	18006	197
82319	CDH86	200	Foraminifera	18450	80	22072	114
83310	CDH86	200	Organic Carbon	23100	180	27721	246
82324	GGC81	225	Foraminifera	16950	65	20141	92
83315	GGC81	225	Organic Carbon	19550	120	23334	204
82320	CDH86	300	Foraminifera	23900	140	28622	205
83311	CDH86	300	Organic Carbon	25000	180	30032	307
101328	CDH86	350	Foraminifera	23600	80	28285	166
79780	GGC81	390	Foraminifera	22600	130	27153	197
83316	GGC81	390	Organic Carbon	23800	100	28510	176
82321	CDH86	400	Foraminifera	19600	85	23416	147
83714	CDH86	400	Organic Carbon	26200	120	31448	190
101329	CDH86	450	Foraminifera	26400	100	31664	183
82322	CDH86	500	Foraminifera	26700	210	31986	273
83313	CDH86	500	Organic Carbon	28000	310	33365	363
83907	CDH86	600	Foraminifera	25600	150	30798	202
83908	CDH86	700	Foraminifera	33100	190	38498	240
83909	CDH86	800	Foraminifera	34300	260	39666	312
101330	CDH86	900	Foraminifera	38800	490	43680	461

Highlights

- Ti/Ca and Fe/K peaks correspond with Heinrich events
- Ti/Ca and Fe/K peaks are products of intense weathering and increased runoff
- SST was higher, SSS was lower, Nordeste Brazil was wetter during Heinrich events
- Simulated NBC and AMOC transports decrease during North Atlantic cold events